Analytical methods used for the characterisation of specific features of biological tissues related with obesity: A review

Edvardas Brimas,

Rimantas Raudonis,

Aivaras Kareiva[*]

Institute of Chemistry,
Vilnius University,
24 Naugarduko Street,
03225 Vilnius, Lithuania

Obesity has become a global pandemic, leading to the development of many common disorders, such as type 2 diabetes, metabolic syndrome and cardiovascular diseases, and even increases the risk of several cancers. The adipose tissue of obese patients was characterised as a tissue microenvironment composed of adipose tissue macrophages, precursor and hypertrophic adipocytes, and other immune cells that predominantly produce pro-inflammatory cytokines for chronic, low-grade inflammation. In this study, several analytical techniques, such as gas and liquid chromatography, Fourier transform infrared (FTIR) and Raman spectroscopies, nuclear magnetic resonance (NMR) spectroscopy, scanning electron microscopy (SEM) and elemental analysis, were discussed as the main tools used for the characterisation of adipose tissue samples. The emphasis was focused on the relation between the obtained results which provide information about the chemical and structural composition of adipose tissue layers in the human body, as well as main microstructural features and obesity. It was demonstrated that these methods are indispensable tools in order to investigate some special features of human adipose tissue, identifying chemical composition and structural features. Moreover, the summarised results let us to conclude that such characterisation of adipose tissue is an essential step for the possible prediction of the appearance of symptoms of different diseases.

Keywords: adipose tissue, characterisation, gas and liquid chromatography, FTIR spectroscopy, Raman spectroscopy, NMR spectroscopy, chemical analysis, scanning electron microscopy

INTRODUCTION

Obesity is defined as an unhealthy excess of body fat which increases the risk of medical illness and premature mortality, or as a body mass index (BMI) ≥ 25 kg/m² and ≥ 30 kg/m² for the overweight and obesity thresholds, respectively [1–4]. The obesity prevalence and severity is growing dramatically in many developed and developing countries. Obesity affects >650 million people in the world, according to reports from the World Health Organization. In the European Union (EU), the levels of obesity and overweight have been rising as well in the last decades [5–7]. Obesity has been clearly associated with numerous pathophysiologic processes and co-morbidities, such as metabolic syndrome (MetS), type 2 diabetes mellitus (T2DM), cardiovascular disease (CVD) and most types of cancer which is the most common cause of death in the western world [8–10]. Most of the adult obese population will have fatty liver, and approximately one-third will develop non-alcoholic fatty liver disease [11].

* Corresponding author: Email: aivaras.kareiva@chgf.vu.lt

There are three types of adipocytes: white, brown and brite (brown in white, also known as beige) adipocytes. Briefly, white adipose tissue (WAT) is the main tissue for storing energy. Under conditions of energy surplus, lipids are stored as triglycerides and can then be released as fuel under conditions of negative energy balance. Brown adipose tissue (BAT) is responsible for non-shivering thermogenesis, essentially converting stored lipids into heat through fatty acid oxidation. The function of brite adipocytes is less well characterised, but they have a phenotype intermediate between white and brown adipocytes. They differ in their appearance, morphology, function, and gene expression profile [12, 13]. The adipose tissue can also be classified according to its location in the human body (see Fig. 1 [14]). Subcutaneous adipose tissue (SAT) is the fat just under the skin. Preperitoneal adipose tissue (PAT) is located prior peritoneum. Visceral adipose tissue (VAT) surrounds organs interfering the function of organs. Moreover, there is conflicting information about differences between the fatty acid composition of subcutaneous adipose tissue, preperitoneal adipose tissue and visceral adipose tissue. Varying proportions of fatty acids from adipose tissue may be related to specific diseases as well [14].

Adipose tissue is generally considered as a storage depot for excess energy, which is stored as triglycerides. It was long considered as a passive organ, but the adipose tissue has been described as an endocrine organ recently with important physiological roles [15]. Adipose tissue, which is primarily composed of adipocytes as well as pre-adipocytes, macrophages, endothelial cells, fibroblasts and leucocytes, has been increasingly recognised as a major player of systemically metabolic regulation [16, 17]. There is conflicting information about differences between the fatty acid composition of SAT and VAT. Varying proportions of fatty acids from adipose tissue may be related to atherosclerosis, MetS, T2DM, CVD and other diseases and might exert a direct influence on serum lipids that may differ depending on the adipose tissue region [11, 18]. During cancer development, loss of total adipose tissue occurs in most cancer patients [19]. However, obesity related with metabolic disturbances varies widely among obese individuals. For example, as opposed to the extent of SAT, the increase in VAT is associated with increased metabolic disturbances and CVD. An individual with a normal BMI but with an increased VAT is at higher risk of developing metabolic disturbances than an obese person with less VAT [20]. However, loss of total adipose tissue did not reflect changes in SAT and VAT in the same direction or intensity. The adipose tissue distribution during pregnancy showed a tendency towards a decreased accumulation of subcutaneous and increased accumulation of preperitoneal adipose tissue [21]. The relationship between obesity, namely PAT and arterial stiffness in adults and
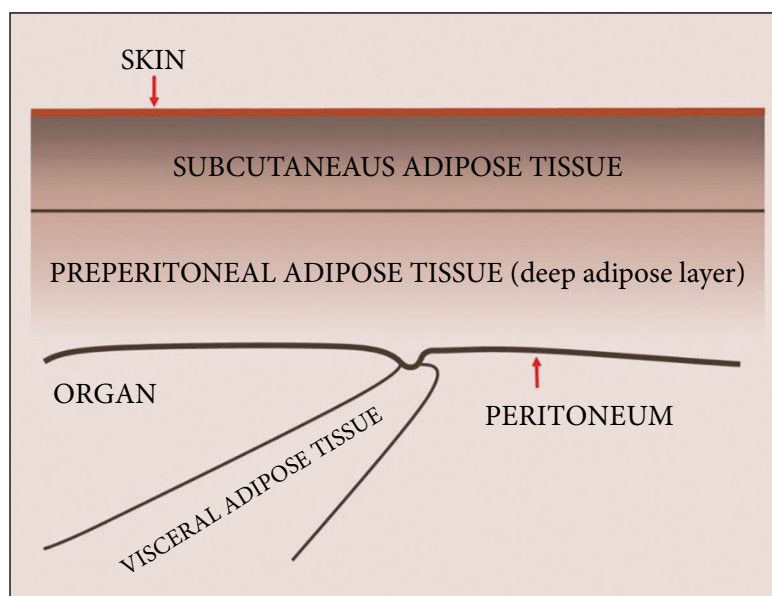

Fig. 1. A schematic diagram of adipose tissues in human body [14]

in children, has been also reported [22–24]. It was found that PAT volume was increased in people with chronic major depressive disorder versus those with acute major depressive disorder or controls [25]. The hypothesis that the ratio of visceral to subcutaneous adipose tissue is associated with altered sepsis outcome was recently partially proved [26]. The relationship between VAT and sugar-sweetened beverage intake was also determined [27]. Several studies showed the strongest correlation between the symptoms of different diseases and changes in VAT mass [28–31]. For example, Brown et al. [32] determined that VAT is correlated with a variety of biomarkers related to glucose homeostasis, inflammation, and lipid metabolism. Moreover, the quality and quantity of VAT play significant roles in adipocyte function and are related to insulin resistance [33]. It was also concluded about the existence of a strong correlation between glucose production and insulin sensitivity in SAT [34].

Although the development of obesity is easily attributed to excess intake of calories, the underlying reasons for the metabolic disturbances and health risks associated with obesity are still unclear. Though an association between obesity and health problems is well established, the link may-in reality-not be as simple. In fact, findings from experimental animal models and human studies collectively suggest that the increased morbidity in obesity is mainly due to increased levels of circulating lipids resulting in ectopic lipid deposition and lipotoxicity, which in turn negatively impacts metabolism and tissue function, suggesting dyslipidemia as the primary inducer of disease development [35–38]. To determine the link between obesity and metabolic syndromes, researchers are studying a wide variety of adipose tissue features, changes of different parameters, and various physical properties in obese people; examine the chemical composition of adipose tissue, the change in composition depending on the progression of the disease and treatment [39–59]. The abundance of various parameters is set so that it is not easy to see and capture the desired connection and it is not always possible. Not only physicians but also chemists, biochemists, physicists and materials scientists are actively involved in these studies. The following main methods are currently used to characterise adipose tissue: gas and liquid chromatography, FTIR, Raman and NMR spectroscopies, scanning electron microscopy (SEM), elemental analysis using sensors and other techniques. The main aim of this review is to introduce the scientific community with the possibilities of using these latest methods of instrumental analysis in the study of the peculiarities of human adipose tissue.

GAS AND LIQUID CHROMATOGRAPHY

The conventional methods for determining the composition of fats in the adipose tissue are gas and liquid chromatography [60–63]. Walters et al. [64] stated that the recent obesity epidemic in children also showed an increase in the prevalence of hypertension. As blood pressure (BP) is associated with (long-chain) polyunsaturated fatty acids (LC PUFA), the authors investigated the direct and indirect effects on the PUFA level, body mass index (BMI) and BP. Whole blood fatty acids were measured by a validated gas chromatographic method and recorded as percentage of weight of all fatty acids detected. Gas chromatography-tandem mass spectrometry (GC-MS) was used for the determination of 209 polychlorinated biphenyl in the human adipose tissue [65]. For decades, these compounds are extensively used in industry, are very biostable, lipophilic and resistant to both chemical and biological degradation that tend to accumulate in different tissues of organisms. GC-MS was also used to analyse the isomers of monounsaturated fatty acid having sixteen carbon atoms (16:1) in human adipose tissue (see Fig. 2) [66]. It was reported that human phagocytic cells also expressed low levels of a third 16:1 isomer, sapienic acid [16:1n-10 (cis-6-hexadecenoic acid)]. Despite the common assumption that 16:1n-10 is restricted to humans, the authors found relatively high levels of this fatty acid in murine macrophages and also in murine macrophage-like cell lines. Poskus et al. [67, 68] successfully applied a silica-based silver ion solid-phase extraction (Ag$^+$-SPE) for the fractionation and subsequent gas chromatographic analysis of trans fatty acids in human adipose. In the work [69], the samples of adipose tissue and serum were obtained from 386 subjects undergoing non-cancer-related surgery and were extracted using validated methodologies. Residues of persistent organic pollutants
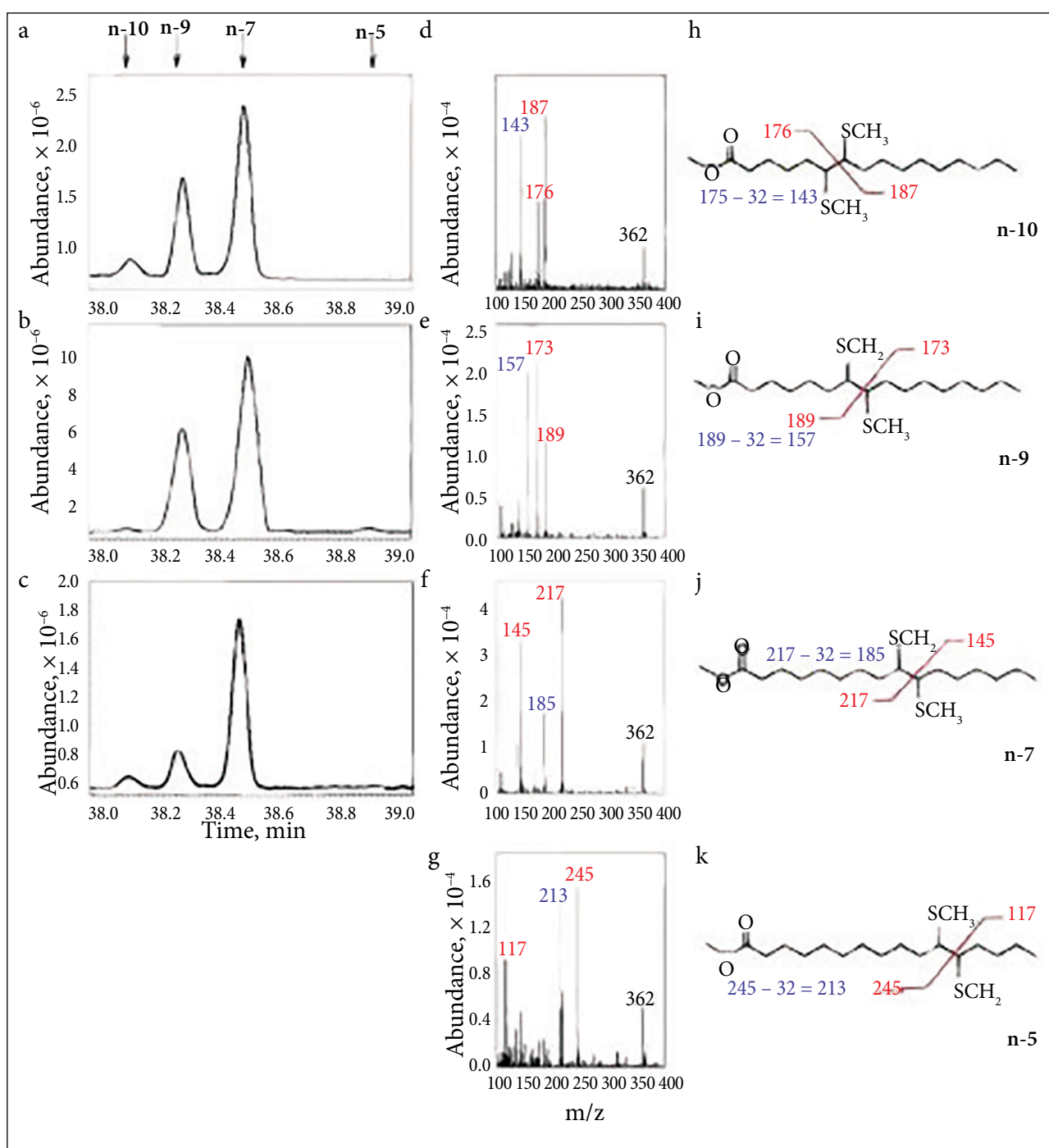
Fig. 2. Analysis of 16:1 isomers in human cells. After sample collection and lipid extraction, total lipids were transmethylated. The resulting fatty acid methyl esters were derivatised with DMDS and DMDS adducts of 16:1 isomers measured by GC/MS. Chromatographic region showing the main 16:1 fatty acid isomers present in human monocytes (a), human monocyte-derived macrophages (b) and human serum (c). The mass spectra corresponding to the **n-10** (D, H), **n-9** (E, I), **n-7** (F, J), and **n-5** (G, K) isomers, indicating the molecular ion (M+) and the three diagnostic peaks (fragment corresponding to the terminal methyl part of the molecule, the fragment containing the carboxyl group, and the latter with the loss of methanol) are also shown [66]

were analysed by means of high-resolution gas chromatography with a mass spectrometry detector in a tandem mode. The possible association of concentrations of persistent organic pollutants in the human body with the prevalence of type 2

diabetes was determined in samples of adults from Southern Spain.

In the work [70], the total fatty acids extracted from red blood cells and arachidonic acid-to-eicosapentaenoic acid (AA-to-EPA) ratios were assessed

using GC-MS assay in a single-ion monitoring mode. The study was conducted on 64 male rats. It was concluded that anti-inflammatory drugs (e.g. celecoxib) and antioxidants (e.g. safranal) appeared as promising pharmaceutical and nutritional alternatives, respectively, that can prevent or reduce lipotoxicity-associated metabolic disturbances. The gas chromatography was also used to study the quality (oxidative stability), fatty acids profile and their distribution in triacylglycerol (TAG) molecules of fat obtained from the adipose tissue of wild boar, badger and wild goose [71]. The determination of fatty acids in milk using a new thin layer chromatography and gas chromatographic (TLC-GC) techniques was performed [72]. The results obtained confirmed the applicability of TLC-GC as a new method, not requiring blood sampling, that could be incorporated into the daily milking routine. The applicability of this method could allow the implementation of nutritional and management strategies in order to avoid the development of metabolic diseases.

Liquid chromatography techniques are also very important in lipidomics research [73]. For instance, antibiotic levels in the adipose samples were determined with reverse phase high-pressure liquid chromatography (HPLC) [74]. The aim of this study was to evaluate the concentration of cefazolin in adipose tissue of patients undergoing bariatric surgery. An inverse correlation between BMI and concentration of cefazolin in adipose tissue was observed. Bartosinska et al. [75] developed the HPLC method for the quantitative determination of tocotrienols in human breast adipose tissue (Fig. 3). In the work [76], ultra-performance liquid chromatography (UPLC) coupled with electrospray ionisation (ESI) mass spectrometry (MS) were employed for the comprehensive qualification and quantification of triacylglycerols (TGs) with a specific fatty acid chain composition in human plasma and liver tissues including hepatocellular carcinoma and para-carcinoma tissues. Multiple MS detection modes from QTRAP MS and FT-ICR MS
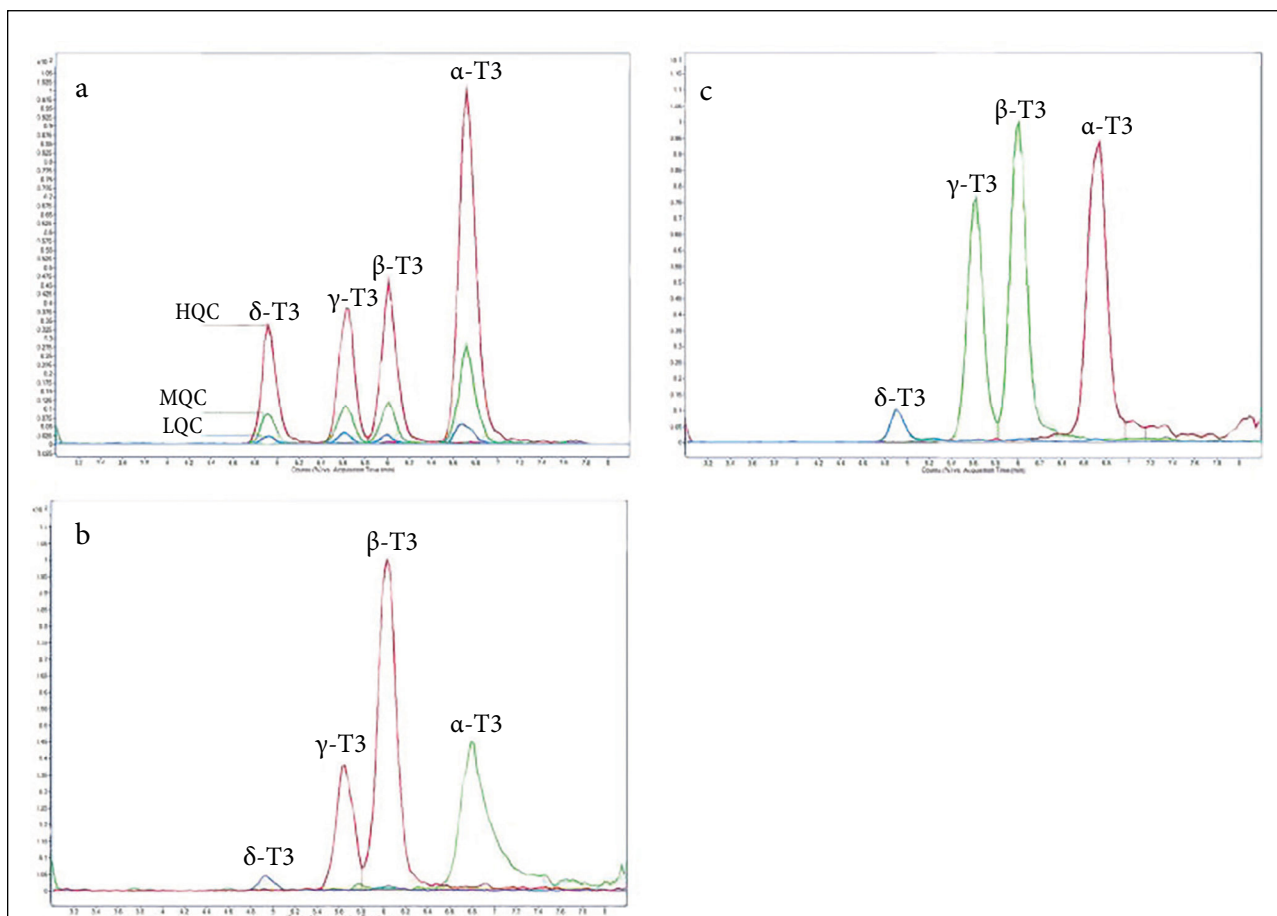

Fig. 3. Chromatographic separation of tocotrienols: (a) quality control (QC) samples of tocotrienol standard solutions; (b) extract of breast adipose tissue pooled homogenate; (c) an exemplary chromatogram of the extract obtained from patients' breast adipose tissue sample [75]

were utilised, and hundreds of TG species (including many oxidised TG species) with their specific fatty acid chain compositions have been qualified and quantified. It was concluded that the developed analytical procedure is of significance for an accurate analysis of these lipids. Recently, liquid chromatography approaches were used to evaluate different obesity models by determining different analytes in adipose tissue of rats [77, 78]. The main information regarding application of gas and liquid chromatography for the analytical characterisation of biological tissues related with obesity is summarised in Table 1.

FTIR AND RAMAN SPECTROSCOPIES

Buckus et al. [79] demonstrated that FTIR spectroscopy could be used for the analysis and direct qualitative characterisation of adipose tissue composition. According to the results of FTIR analysis it was concluded that the main functional groupings in the adipose tissue of different obese patients were the same; however, the real chemical composition of the samples obtained from subcutaneous, preperitoneal and visceral layers of adipose tissue from different patients was different. The representative spectra recorded for the different specimens are shown in Fig. 4. The FTIR spectra of adipose samples obtained from different patients and different tissues contain broad and sharp bands located at 2950–2800 cm^{-1} as well as weaker bands centred at around 3150, 1350 and 900 cm^{-1}. These bands correspond to the n(C-H) stretching vibration of methylene and alkyl groups [79]. The sharp and intensive absorption band located at 1743–1710 cm^{-1} is attributed to the stretching vibrations

Table 1. **Application of gas and liquid chromatography for the analytical characterisation of biological tissues related with obesity**

| Method	Analyte	Matrixe	Reference
Gas-liquid chromatography	Long-chain fatty acids	Synthetic samples	[60]
Rapid gas-liquid chromatography	Fatty acids	Blood samples of over-weight and obese children	[64]
Gas chromatography coupled with tandem mass spectrometry	Caffeine, yamemazine, meprobamate, morphine and 6-monoacetylmorphine	Adipose tissue of human samples from a real autopsy case	[62]
Gas chromatography coupled with mass spectrometry	Fatty acids isomers	Human monocytes isolated from buffy coats of healthy volunteer donors	[66]
Gas chromatography coupled with mass spectrometry	Organochlorine pesticides and polychlorinated biphenyls	Human adipose samples	[69]
Gas chromatography coupled with tandem mass spectrometry	Fatty acids	Red blood cells of rats	[70]
Gas chromatography	Trans fatty acids	Human adipose samples	[67, 68]
Gas chromatography	Fatty acids	Adipose of wild animals	[71]
Thin layer chromatography and gas chromatography	Fatty acids	Milk of dairy cows	[72]
QSRR model to predict gas chromatographic retention times	Polychlorinated biphenyls	Human adipose tissue	[65]
Reverse phase high-pressure liquid chromatography	Cefazolin	Human adipose tissue	[74]
High-pressure liquid chromatography	Tocotrienols	Human breast adipose tissue	[75]
Ultra-performance liquid chromatography	Triacylglycerols	Horse adipose tissue	[76]
High-performance liquid chromatography	The trypsin inhibitor purified from tamarind	Adipose of rats	[77]
Liquid chromatography-tandem mass spectrometry	5-Amino-1-methyl quinolinium	Rat plasma and urine samples	[78]
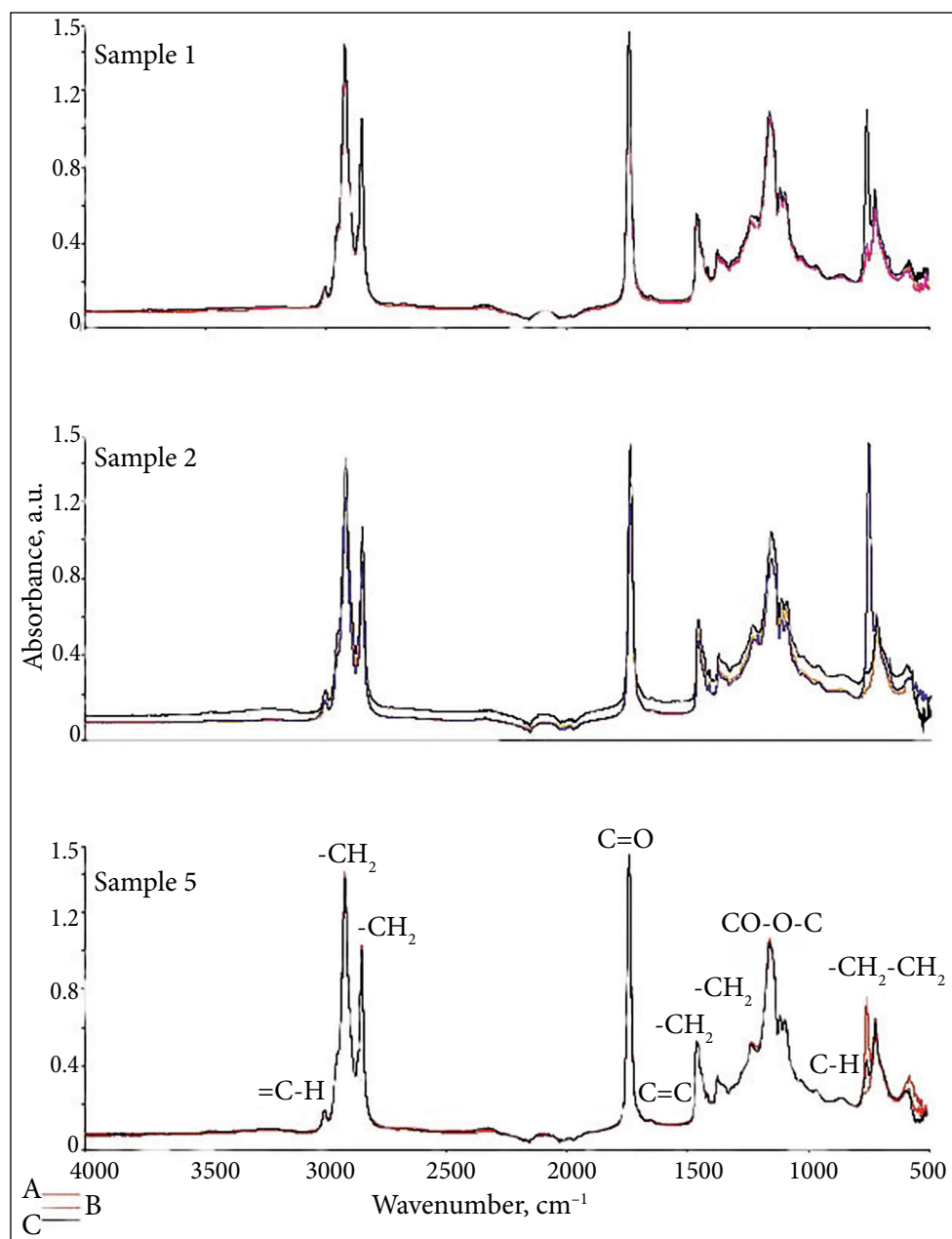
Fig. 4. FTIR spectra of adipose tissue samples taken from different layers of adipose tissue of three patients [79]. Subcutaneous (a), preperitoneal (b) and visceral (c) layers of the adipose tissue of three patients

of C=O in a triacylglycerol functional group [79]. FTIR spectra of all samples contain the same bands located at 1680–1600 cm^{-1} and 1200–1000 cm^{-1} which correspond to C=C and CO-O-C vibrations, respectively. These observations let us to state that unsaturated bonds in the fatty acids and esters are present in the investigated samples. The broad bands centred at ~800–700 cm^{-1} correspond to the –CH$_2$-CH$_2$– vibrations in long alkyl chains. Interestingly, the intensity of these bands is quite different in the spectra for different adipose samples. This only one slightly different observation is vis-

ible in all FTIR spectra confirming the presence of different fatty acids in the adipose tissues.

The similar conclusions were made by other authors as well. The FTIR results of the studies [80, 81] demonstrated that there were several alterations in the triglyceride spectral region of SAT and VAT of male obese mice. The authors [82] have used FTIR spectroscopy to investigate the composition of fatty acid of adipose tissue in men having the metabolic syndrome. The results from the patients with uronephrolithiasis differed from the results from the control group. Irrespective of MS diagnosis,

all individuals with kidney stones had significantly higher percentages of monounsaturated fatty acids and lower percentages of polyunsaturated fatty acids than did healthy individuals. A very interesting observation was demonstrated by Ami et al. [83]. They showed that ATR-FTIR spectroscopy, coupled with multivariate analysis, can differentiate adipose tissue aspirates containing amyloid deposits from unaffected samples with a high sensitivity and specificity. Moreover, this approach was rapid and required no sample processing besides blood removal.

ATR-FTIR combined with chemometrics were used for the estimation of postmortem interval in the adipose tissue of mice [84]. This study showed that adipose tissue is a promising option for estimating later stages in the postmortem interval but temperature has a great influence on the postmortem changes in adipose tissue. The importance to use the cryostat technique to make thin sections of biological samples for FTIR microspectroscopy imaging was also shown by Liyanage et al. [85]. It was demonstrated that FTIR spectroscopy is a very useful tool in the development of alternative tissues for liver transplantation. In the procedure of the preparation of porcine livers, FTIR spectroscopy was used to control the presence of nuclear material and the detergent residue in the samples could be used for liver transplantation [86]. FT-IR spectroscopy proved to be an accurate technique for detecting and quantifying the amount of lard taken from the adipose tissue of pigs and mixed with sunflower, canola, coconut, olive, and mustard oil. The results were comparable to the concentration of lard in binary mixtures with other oil. The correlation coefficient of 0.9577 was produced in the wavenumber region of 1078.01–1246.75 cm^{-1} [87].

It was shown that Raman spectroscopy can be used as a simple, fast and non-destructive method for the quantitative analysis of Omega-3 fatty acids in fish oil supplements [88, 89]. Raman spectroscopy is one of the vibrational spectroscopies. One of the great advantages of Raman spectroscopy is that it is less invasive; a sample can be studied *in situ* using laser light without pre-treatment [89]. These advantages make Raman spectroscopy possible for large-scale detection and analysis for fat content and fatty acids [90].

Raman spectroscopy for the characterisation of adipose tissue samples obtained from human adipose tissue for the first time was used by Yanina et al. [91]. The enzymatic destruction of adipose tissue by encapsulation of lipase into the polymeric microcapsules has been investigated. Raman spectra of adipose tissue before and after lipase treatment were acquired 100 and 40 times, respectively, from different spatial points of the tissue. Figure 5 shows the normalised averaged spectra of both tissue samples. The development of Raman imaging probes for intraoperative cancer surgery guidance, the approach used in Refs. [92, 93], had a great potential to improve minimally invasive procedure performance with an endoscope or surgical robots. Both of those technologies are currently using an imaging bundle to recreate white-light images of the tissue from which the surgeon guided himself through the tissue. The confocal Raman microspectroscopy was applied for the simultaneous visualisation, identification and quantification of the lipid accumulation in lipid droplets of aggressive human breast cancer cells derived from overweight and obese patients [94]. It was demonstrated that this technique enables imaging of cell compartments as well as quantification and monitoring of specific biomolecules and metabolic processes on a single cell level. Moreover, a significant increase in unsaturation, esterification and the lipid to protein ratio in lipid droplets in breast cancer cells incubated was identified using a Raman microspectrosopy method. The same method was successfully applied to evaluate the effect of hyperglycemia on proliferating, differentiating and maturating human visceral pre/adipocytes [95].

The Raman spectroscopy was also used to investigate molecular compositions of lipid droplets changing in live hepatic cells stimulated with major fatty acids in the human body, i.e. palmitic, stearic, oleic and linoleic acids [96]. Majka et al. [97] developed a novel strategy of studying perivascular adipose tissue in human vessels with the application of fiberoptic Raman spectroscopy and spectral modelling. The study showed the results of the investigation of a group of 10 male patients of age 57–73 with advanced atherosclerosis. All patients were diagnosed with coronary artery disease and were subjected to coronary artery bypass surgery. All patients showed hypercholesterolemia and hypertension, and some of them suffered from other co-morbidities; in particular, 6 had confirmed type 2 diabetes mellitus. It was confirmed that the proposed method for the reliable and rapid evaluation of the phenotype of perivascular adipose tissue in the future can be adopted intraoperatively in hospital conditions.
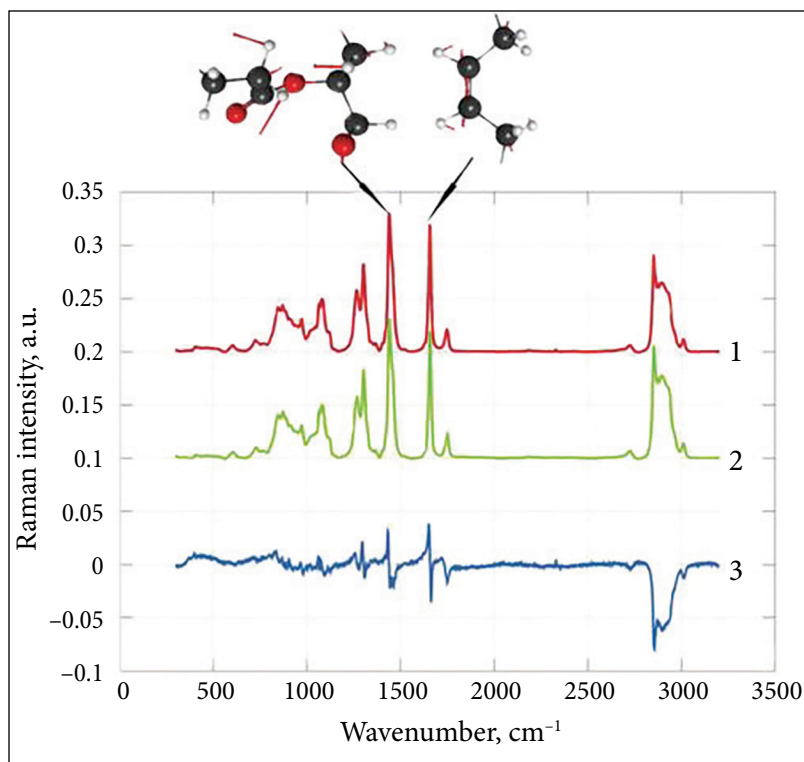
Fig. 5. Normalised Raman spectra: (1) the average of 40 collected spectra of adipose tissue after lipase treatment; (2) the average of 100 collected spectra of adipose tissue before treatment; and (3) calculated difference spectrum ($\times 5$) for two averaged Raman spectra shown above. Computed molecular models at the top represent parts of a TG molecule, where white, black and red spheres are H, C and O atoms, respectively. Red arrows show vibrational modes of this molecule which correspond to 1439, 1456 and 1657 cm^{-1} peaks in the Raman spectra of adipose tissue [91]

The study [98–101] demonstrated the feasibility of using fiber-optic Raman spectroscopy in the quantitative analysis of specific fats in the body in a totally non-invasive manner. Golden Syrian hamsters, different rat groups and pork were used as adipose tissue sources. Confocal Raman microscopy was used to record horse fat depth profiles measuring the unsaturation degree [102]. It was noted that the presence of proteins in the studied horse fat was found in the first layer of the tissue, that is, very close to the skin. The Raman spectroscopy was used to detect changes in adipose tissue associated with a prolonged intake of desloratadine, a commonly used second generation antihistamine to treat allergic reactions [103]. White and brown adipose tissue samples were excised from adult rats. The Raman spectra indicated that antihistamine use reduces the protein-to-lipid ratio in the brown adipose tissue but not the white adipose tissue, indicating that the effect on adipose tissue is location-dependent.

It was recently showed that Raman spectroscopy results provided new insights into the genetics of fatty acid traits in rainbow trout [104]. Many biomedical applications require measurements of Raman spectra of tissue under ambient lighting conditions. However, the background light often swamps the weaker Raman signal. The use of time-gated (TG) Raman spectroscopy based on a single photon avalanche diode (SPAD) operating in time-correlated single photon counting and near-infrared laser excitation was investigated for the acquisition of Raman spectra and spectral images of biological tissue in study [105]. Advances of Raman spectroscopy investigating metabolic syndrome was also observed in the review article [106]. Thus, Raman spectroscopy is a powerful analytical technique for the analysis of tissue and has been widely used for medical applications. Several Raman devices have also been tested in hospitals for improving diagnosis. Confocal Raman microscopy analyses might function as a valuable diagnostic tool to identify metabolic

alterations in biological samples which in turn could provide more detailed insights in the pathogenesis of breast cancer in association with obesity. The main information regarding the application of FTIR and Raman spectroscopies for the analytical characterisation of biological tissues related with obesity is summarised in Table 2.

NMR SPECTROSCOPY

The ^{1}H NMR spectroscopy analysis could also provide metabolic information indicating disturbed glucose metabolism, fatty acid metabolism, amino acid metabolism and activated inflammatory response in patients [107]. However, the ^{1}H NMR spectra of adipose tissue samples taken from different obese patients were rather similar [79]. Thus, according to these results, the disease symptoms observed for these patients might be also similar. However, the authors also identified some characteristic features in each ^{1}H NMR spectrum. Based on the integral values of the ^{1}H NMR spectra the composition of adipose tissue was estimated on two classes of fatty acids: unsaturated and saturated. It was suggested that patients with metabolic disorder had a lower level of polyunsaturated and a high level of monounsaturated fatty acids in the adipose tissue.

A simple method to detect gluconeogenesis from glycerol in obese humans was developed [108]. For the first time in obese humans, a simple stable isotope technique to investigate *in vivo* the mechanisms underlying the effects of excess visceral adiposity on gluconeogenesis from glycerol was used. Glycerol-gluconeogenesis was evaluated by determining the fraction of ^{13}C enrichment in blood glucose using the NMR spectroscopic quantification of ^{13}C-labelled glucose isotopomers. The findings provided a preliminary evidence that excess visceral fat disrupts multiple pathways in hepatic gluconeogenesis from glycerol. The differences in T2 relaxation times between the CH_2, CH_3 (non-omega-3) and n-3 CH_3 (omega-3) signals enabled the identification of well-resolved n-3 CH3 resonances, making the developed method suitable for the direct detection of n-3 fatty acids at 7 T [109]. This work proposed a relatively simple approach for the reliable estimation of the n-3 FA fraction, *in vivo*, in a samples of healthy volunteers.

It was shown that the common shared lipid accumulation mechanism in lipoma is a reduction in lipolysis [110]. 15 patients (12 males and 3 females; age range 26–79 years; normal BMI) with single superficial subcutaneous lipomas were recruited. ^{1}H NMR spectra were corrected for baseline and phase distortions and calibrated using the residual proton resonance of methanol at 3.49 ppm. The lipid composition of the samples was determined by integrating the methyl (0.9 ppm), allylic (2.7 ppm), olefinic (5.3 ppm) and vicinal-olefinic (2.0 ppm) resonances. Superficial lipomas could thus be used as a model for lipid accumulation through altered lipolysis as found in obese patients. It is well known that the synthesis and turnover of triglyceride in adipose tissue involves enzymes with preferences for specific fatty

Table 2. **Application of FTIR and Raman spectroscopy for the analytical characterisation of biological tissues related with obesity**

Method	Analyte	Matrixe	Reference
FTIR spectroscopy	Fatty acids	Human adipose samples	[79]
FTIR spectroscopy	Triglycerides	Adipose of mice	[80]
FTIR spectroscopy	Protein to lipid ratio	Adipose of mice	[81]
FTIR spectroscopy	Fatty acid methyl esters	Men adipose samples	[82]
FTIR spectroscopy	Abdominal fat aspirates	Human adipose samples	[83]
Raman spectroscopy	Fatty acids	Fish oil supplements, food	[88, 89]
Raman microspectroscopy	Lipid droplets	Human breast cancer cells; visceral adipocytes; hepatic cells	[94, 95, 96]
Raman spectroscopy	Carotenoids and lipid unsaturation	Human adipose of the internal mammary artery	[97]
Raman spectroscopy	Trilinolein and tricaprin	Hamsters adipose tissue	[98]
Raman spectroscopy	Lipids	Adipose of rats	[99, 101]
Raman spectroscopy	Fatty acids	Rainbow trout	[104]

acid classes and/or regioselectivity regarding the fatty acid position within the glycerol moiety. The focus of the study [111] was to characterise both the composition of fatty acids and their positional distribution in triglycerides of biopsied human subcutaneous adipose tissue, from subjects with wide ranges of the body mass index (BMI) and insulin sensitivity, using ^{1}H and ^{13}C NMR spectroscopy. Chloroform extracts of the adipose tissue biopsies yielded ^{13}C and ^{1}H NMR spectra with a good resolution of triglycerides fatty acid hydrogens and carbons, as shown by Fig. 6. The examination of the fatty acid ^{13}C NMR
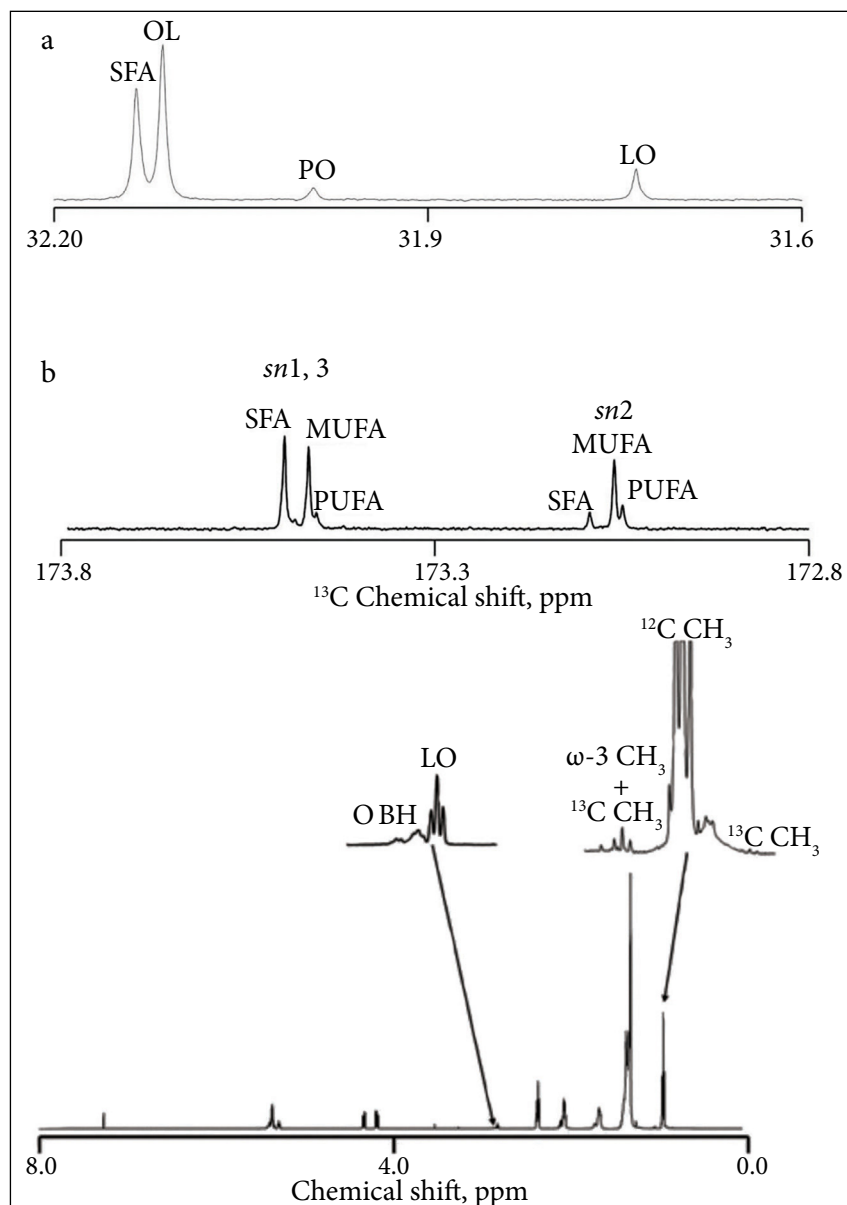

Fig. 6. Expanded portions of a ^{13}C NMR spectrum obtained from a 21.7-mg adipose tissue biopsy sample (at top). Signals of the ω-3 carbons for saturated fatty acids (SFA), oleic acid (OL), palmitoleic acid (PO) and linoleic acid (LO) are shown in (a), while those representing SFA, monounsaturated fatty acids (MUFA) and polyunsaturated fatty acids (PUFA) distributed between the sn1,3 and sn2 carboxyls are shown in (b). The corresponding ^{1}H NMR spectrum of the sample with the fatty acid methyl signals of ω-3 polyunsaturated fatty acids (ω-3 CH$_3$) and those of all other fatty acids (^{12}C CH$_3$), including their ^{1}H-^{13}C−coupled satellites from ^{13}C natural abundance (^{13}C CH$_3$) (at bottom). Also highlighted are the linoleic acid bisallylic hydrogens (LO). The poorly defined multiplet component upfield of LO represents other bisallylic hydrogens (OBH) from other species of polyunsaturated fatty acids [111]

signals from both human adipose tissue biopsies, as well as the triglycerides standard mixture, revealed that the ω-3 signals, whose chemical shifts are centered at 31.9 ppm, provided a superior resolution of the most abundant fatty acid species compared with the ω-2 signals that were used previously. The ^{13}C NMR spectra of individual glyceryl trimyristate, glyceryl tripalmitate and glyceryl tristearate standards showed identical chemical shift values for the ω-3 position. Returning to the human study cohort, the data revealed that subtle alterations in the distribution of MUFA and PUFA between the sn1,3 and sn2 sites of glycerol were associated with BMI, independent of their total abundance. These data were consistent with differences in fatty acid selectivity by one or more enzymes involved in triglycerides metabolism and/or different triglycerides-fatty acid cycling activities in the setting of obesity.

The variation in the metabolic profile of breast cancer focusing on lipids as triglycerides and free fatty acids that may alter in malignant breast tissues and lymph nodes from adjacent benign breast tissues was evaluated by ^{1}H NMR spectroscopy [112]. The ^{1}H NMR spectra were recorded on 173 tissue specimens comprising of breast tumour tissues, adjacent tissues, few lymph nodes and overlying skin tissues obtained from 67 patients suffering from breast cancer. Reduction in the lipid content was observed in malignant breast tissues along with a higher fraction of free fatty acids. This study may help in future for a precise evaluation of the lipid classification including small molecules as a source of early diagnosis of invasive ductal carcinoma by employing *in vivo* magnetic resonance spectroscopic methods.

Non-invasive ^{1}H NMR spectroscopy was used to monitor the hepatic lipid content and fatty acid composition *in vivo* [113]. Male (N = 10) and female (N = 10) mice were used for the animal experiments. The authors detected higher amounts of omega-3 in total liver lipids of female than male mice. Phenelzine-treated mice exhibited a lower body fat content, subcutaneous adipose tissue mass and lipid content in skeletal muscles than the control, without the decreased body weight gain or food consumption [114]. Mice were fed a standard chow and given phenelzine in drinking water for 12 weeks. The body composition was determined by NMR spectroscopy. ^{1}H, ^{13}C and ^{31}P NMR spec-

troscopies were used to investigate different health problems related with obesity performing animal experiments with male rats [115] and adipose tissue of mouse [116, 117]. High resolution magic angle spinning NMR spectroscopy was successfully used for the qualitative study of the highly specialised lipid tissues of cetaceans [118]. The HR-MAS NMR spectra of the representative samples are presented in Fig. 7. Assignment of the major peaks detected by HR-MAS NMR in the blubber and melon of the harbour porpoise and long-finned pilot whale, and calculations used to determine peak area are presented in Table 3.

A new NMR-based method was developed, which allows, in addition to the determination of the relative fatty acyl composition, the assignment of unsaturated fatty acyl residues to the positions of the glycerol backbone [119]. Standard ^{1}H NMR as well as ^{13}C NMR spectra were recorded from the solutions of pure triacylglycerols of known compositions and different vegetable oils (olive, garlic, sesame, corn, sunflower, walnut and linseed). However, it was concluded that this approach is not a suitable method for the trace analysis.

It was investigated how rapid weight loss due to a very low calorie diet affects the fecal microbiota and fecal bile acid composition [120]. To support the explanation of obtained results, the urine metabolic phenotypes were measured by ^{1}H NMR spectroscopy. The investigations of the interaction between microbiota and adipose tissue physiology in humans occur very intensively. And ^{1}H NMR spectroscopy plays a very important role in these investigations [121, 122]. The main information regarding the application of NMR spectroscopy for the analytical characterisation of biological tissues related with obesity is summarised in Table 4.

ELEMENTAL ANALYSIS

Human body lipids serve as a harbour for various organic substances, they may absorb different metabolic products, and they have different calorific capacity depending on their location and forms. It was demonstrated that atherosclerotic plaque contains not only organic but also inorganic elements [123]. For the determination of sodium and calcium ions, atomic adsorptive spectrometry (AAS) was used. Figure 8 shows that the content of Ca is relatively higher in AP (loose) than AP (dense), and the ratio

Table 3. **Assignment of 24 major peaks detected by HR-MAS NMR in the blubber and melon of the harbour porpoise and long-finned pilot whale, and calculations used to determine peak area**

| Peak	$^1H\ \delta$(ppm)	Assignment		Component moiety	Area value
a	0.87	Terminal methyl function	CH_3	Long linear FA chains (except ω3)	$= \alpha(a, s) - \alpha(s) = A(a, s) - \hat{A}(s) = A(a, s) - 3*A(t)$
b	0.93 (d, $^3J_{HH} = 6.6$ Hz)	Isopropyl methyl	$(CH_3)_2\text{-}CH\text{-}CH_2\text{-}CO\text{-}O\text{-}$	IVA chain	$= 3*(\alpha(j) + \alpha(v)) = 3*(A(j) + A(v))$
c	0.93 (d, $^3J_{HH} = 6.6$ Hz)	Terminal methyl function	$CH_3\text{-}CH_2\text{-}CH =$	ω3 chains	$= \alpha(b, c) - \alpha(b) = A(b, c) - \hat{A}(b) = A(b, c) - (3*(A(j) + (v)))$
d	1.13	Isopropyl methyl	$(CH_3)_2\text{-}CH\text{-}CO\text{-}O\text{-}$	IBA chain	measured directly (but impossible to separate from peak x)
e	1.26–1.32	Methylene	$-(CH_2)_n\text{-}$	All FA chains	measured directly
f	1.53	β-methylene to ester function	$-CH_2\text{-}CH_2\text{-}CO\text{-}O\text{-}$	All FA chains	$= \alpha(f, u) - \alpha(u) = A(f, u) - \hat{A}(u) = A(f, u) - (A(t)/2)$
g	2.02	α-methylene to double bond	$-CH_2\text{-}CH=CH\text{-}$	MUFA and PUFA chains	$= \alpha(g, h, i) - \alpha(h) - \alpha(i) = A(g, h, i) - \hat{A}(h) - \hat{A}(i) = A(g, h, i) - (2/3*\hat{A}(c)) - \hat{A}(i) - A(g, h, i) - 2/3*(A(b, c) - (3*(A(j) + A(v)))) - (A(j) + A(v)/2$
h	2.05	α-methylene to double bond and terminal methyl function	$CH_3\text{-}CH_2\text{-}CH = CH\text{-}$	ω3 chains	$= 2/3\ \alpha(c) = 2/3*(A(b, c) - (3*(A(j) + A(v)))$
i	2.08 (m, $^3J_{HH} = 6.7$ Hz)	Methylene	$(CH_3)_2\text{-}CH\text{-}CH_2\text{-}$	IVA chain	$= \alpha(j) + \alpha(v))/2 = (A(j) + A(v))/2$
j	2.15 (d, $^3J_{HH} = 5.8$ Hz)	α-methylene to ester function	$(CH_3)_2\text{-}CH\text{-}CH_2\text{-}O\text{-}$	IVA chain on glycerol	measured directly
k	2.25	α-methylene to ester function	$-CH_2\text{-}CH_2\text{-}CO\text{-}O\text{-}$	All FA chains	measured directly
l	2.30	α-methylene to ester function	$CH = CH\text{-}CH_2\text{-}CO\text{-}O$	MUFA and PUFA chains	measured directly
m	2.50	α-methylene to ester function	$(CH_3)_2\text{-}CH\text{-}CO\text{-}O\text{-}$	IBA chain	measured directly (but often too weak correct integration)
n	2.77–2.83	Polyunsaturated methylene	$-CH = CH\text{-}CH_2\text{-}CH = CH\text{-}$	PUFA chains	measured directly
o, p	4.07, 4.26	sn-1 and sn-3 esterified glycerol	$-CH_2\text{-}O\text{-}$	Glycerol	measured directly
q	5.20	sn-2 esterified glycerol	$-OCH_2\text{-}CH(\text{-}O\text{-})\text{-}CH_2O\text{-}$	Glycerol	measured directly
r	5.30–5.33	Olefinic hydrogens	$-CH_2 = CH\text{-}$	MUFA and PUFA chains	measured directly
s	0.86 (d, $^3J_{HH} = 6.7$ Hz)	Isopropyl methyl	$(CH_3)_2\text{-}CH\text{-}CH_2\text{-}(CH_2)_n\text{-}$	isobranched long chains	$= 3*\ \alpha(t) = 3*(A(t)$
t	1.15	Methylene	$(CH_3)_2\text{-}CH\text{-}CH_2\text{-}(CH_2)_n\text{-}$	isobranched long chains	measured directly
u	1.51 (m, $^3J_{HH} = 6.6$ Hz)	Methine	$(CH_3)_2\text{-}CH\text{-}CH_2\text{-}(CH_2)_n\text{-}$	isobranched long chains	$= \alpha(t)2 = (A(t)/2$
v	2.17 (d, $^3J_{HH} = 6.9$ Hz)	α-methylene to ester function	$(CH_3)_2\text{-}CH\text{-}CH_2\text{-}CO\text{-}O\text{-}$	IVA chain on WE	measured directly
w	4.00	α-methylene to ester function	$-CO\text{-}O\text{-}CH_2\text{-}$	WE	measured directly
x	1.12	Methyl group	$CH_3\text{-}CH_2\text{-}CH\text{-}(CH_3)\text{-}CO\text{-}O\text{-}$	2MBA	measured directly (but impossible to separate from peak d)
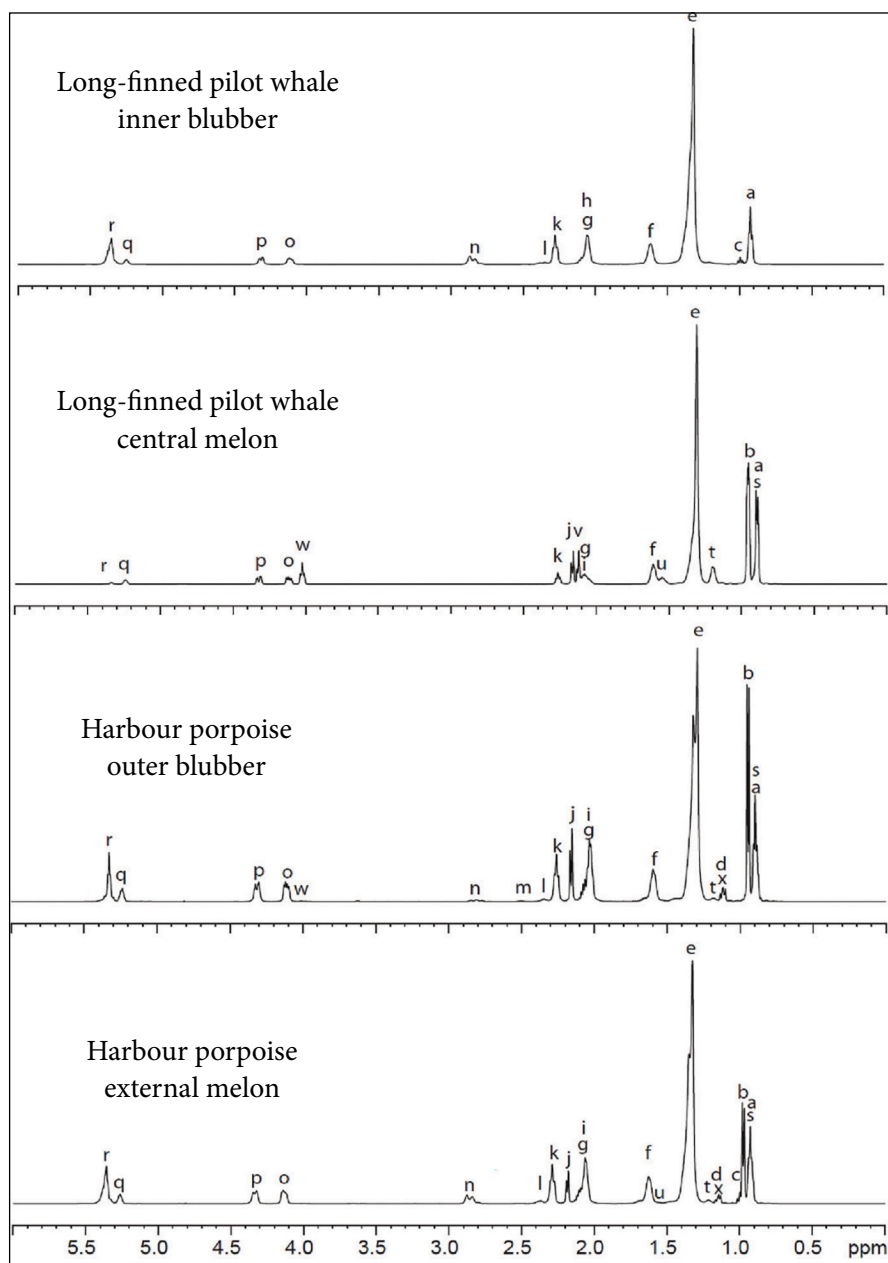
Fig. 7. Representative ^{1}H HR-MAS spectra of the cetacean adipose tissue samples. Intact tissues were placed in a zirconium oxide MAS rotor, D_2O was added for 2 H field locking and ^{1}H HR-MAS NMR spectra were acquired at room temperature (spinning speed = 5000 Hz and ns = 64). The assignment of peaks a to x is given in Table 3 [118]

Table 4. Application of NMR spectroscopy for the analytical characterisation of biological tissues related with obesity

| Method	Analyte	Matrixe	Reference
^{1}H NMR spectroscopy	Fatty acids	Human adipose samples	[79]
^{13}C NMR spectroscopy	Glycerol-gluconeogenesis	Blood glucose	[108]
^{1}H NMR spectroscopy	Lipid composition	Human lipoma	[110]
^{1}H and ^{13}C NMR spectroscopy	Fatty acids	Human subcutaneous adipose tissue	[111]
^{1}H NMR spectroscopy	Triglycerides and free fatty acids	Human breast tumour tissues	[112]
^{1}H NMR spectroscopy	Fatty acids and lipid content	Male and female mice	[113]
^{1}H, ^{13}C and ^{31}P NMR spectroscopies	Body composition	Male rats and adipose tissue of mouse	[115, 116, 117]
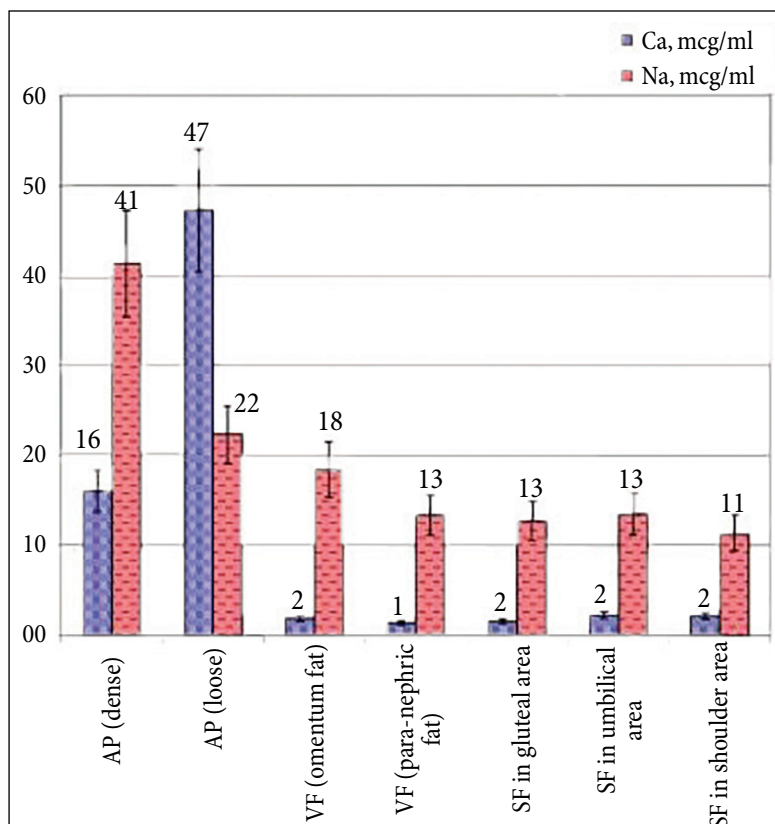
Fig. 8. Calcium (Ca) and sodium (Na) contents in the different anatomical locations of adipose tissue according to elemental analysis ($P < 0.05$; $n = 252$). Abbreviations: AP, atherosclerotic plaque; VF, visceral fat; SF, subcutaneous fat [123]

is a reverse for the Na content. For the determination of the amount of different metals in the adipose samples (Na, K, Mg, Ca, Cr, Mn, Fe, Cu, Zn and Ni) the AAS analysis method was also applied [79]. The results for the determination of selected elements in different layers of adipose tissue obtained from different patients are summarised in Table 5. Evidently, the concentration of sodium and potassium in adipose is much higher in comparison with other elements. The concentration of magnesium is higher in samples 1 and 3, the amount of calcium is very high in sample 1 (267 mg/g). On the other hand, a rather low concentration of calcium was determined in sample 2 (33 µg/g). Evidently, sample 4 contains a higher amount of copper. Interestingly, chromium was found only in the adipose of patients 2 (in all A, B and C layers) and 3 (only in layer A). The concentrations of Fe and Zn do not vary significantly in the adipose tissue samples from different patients. Moreover, Mn and Ni were not detected in all analysed samples of adipose tissue. The relative standard deviation (RSD) values obtained for

the determination of metals in the adipose from the obese patients (6.4–10.3%) indicate a high degree of homogeneity, which could be expected for adipose samples. Moreover, the values obtained are not unusual for such type of analysis and can be considered as suitable for routine analysis. No doubt, the results obtained show various distributions of different metals in the adipose tissue of patients with a different metabolical state. According to the results summarised in this study, the distribution of metal levels in adipose tissue layers is chaotic and does not serve very important information.

The elemental composition in 38 breast tissue samples (19 normal and 19 diseased) was analysed using polarized energy-dispersive X-ray fluorescence (EDX) spectroscopy [124]. The measured elemental concentrations were used in the principal component analysis study to determine the variables that produced the most differentiation between the normal and diseased tissues. The results are summarised in the EDX spectra presented in Fig. 9. Large differences can be seen

Table 5. **Results obtained for the determination of the average amount of metals in adipose tissue from obese patients. Adipose layers: subcutaneous (A), preperitoneal (B) and visceral (C)**

| Sample	Metal	Layer	Amount, mg/g	Layer	Amount, mg/g	Layer	Amount, mg/g
1	Na	A	268	B	404	C	159
	K		160		216		287
	Mg		12.8		16.9		14.4
	Ca		97		73		97
	Fe		19.3		36.8		57.4
	Zn		2.8		4.0		4.4
	Cu		0.26		0.99		0.48
	Cr		–		–		–
2	Na	A	260	B	548	C	365
	K		117		180		153
	Mg		9.9		11.1		8.9
	Ca		11.39		18.86		2.83
	Fe		28.5		53.1		18.6
	Zn		2.1		6.3		2.8
	Cu		0.50		0.51		1.05
	Cr		3.71		6.34		1.78
3	Na	A	256	B	498	C	278
	K		139		177		119
	Mg		7.8		30.6		13.3
	Ca		8.24		41.60		17.95
	Fe		24.9		29.0		18.8
	Zn		2.5		2.7		2.0
	Cu		0.23		0.20		0.56
	Cr		1.55		–		–
4	Na	A	175	B	198	C	271
	K		334		482		664
	Mg		5.9		11.2		8.7
	Ca		18.6		17.3		7.1
	Fe		30.8		26.6		24.5
	Zn		3.2		3.6		3.1
	Cu		0.42		0.52		2.44
	Cr		–		–		–
5	Na	A	195	B	311	C	143
	K		456		584		294
	Mg		8.5		6.5		3.9
	Ca		21.4		20.5		13.5
	Fe		22.7		32.2		16.8
	Zn		4.6		4.8		3.2
	Cu		0.26		0.52		0.65
	Cr		–		–		–
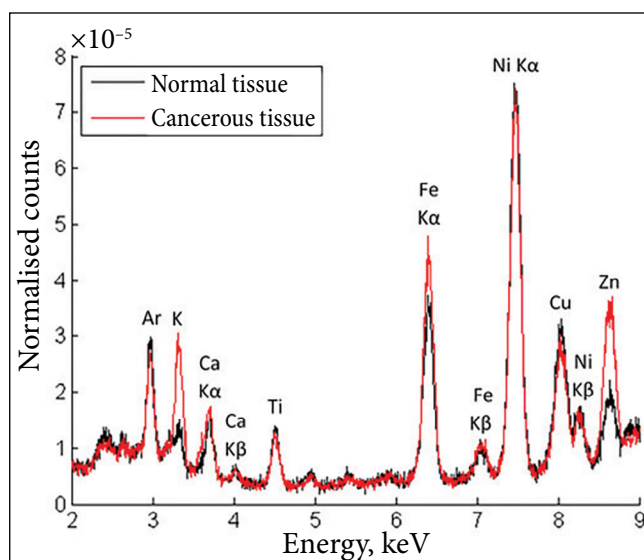
Fig. 9. The average polarized EDX spectra for both the normal (black) and cancerous (red) tissues [124]

in the K, Fe and Zn peaks, with small apparent differences in the Ca and Cu peaks. The Ni and Ti peaks come from contaminants in the measuring system. The adipose tissue from two groups of the patients with obesity (with and without metabolic syndrome) was investigated by means of inductively coupled plasma optical emission spectrometry (ICP-OES) [125]. The main aim of this study was to reveal some differences and regularities in the concentrations of trace elements in the adipose tissue between these two groups of the individuals. Moreover, different types of adipose tissue (subcutaneous, preperitoneal and visceral) were analysed separately in order to investigate distribution of metals between these types in different groups of obese people. Al, Ba, Ca, Co, Cu, Cr, Fe, K, Li, Mg, Mn, Na, Ni, Sr and Zn were selected for the quantitative determination. However, only 6 elements (Na, K, Ca, Fe, Mg and Zn) were determined in all analysed samples independently of the type of adipose tissue and the presence of metabolic disorder of the patient. Concentrations of Ca, Fe, K and Na were found to be strongly dependent on the type of adipose tissue. Other elements in terms of detection frequency in the adipose tissue samples were arranged in the following sequence: Sr (94.7%), Cr (86.2%), Cu (24.6%), Li (18%), Ba (1.8%) and Co (0.05%). The concentrations of Al, Mn and Ni were found to be lower than the limit of detection (LOD) in all analysed samples. In general, there was no ob-

vious difference in the concentrations of metals in the adipose tissue of the patients with and without the metabolic syndrome.

It was predicted that a redox disproportionation develops in some cancers, leading to pools of both more reduced and more oxidised macromolecules compared to normal conditions [126]. This conclusion was made by analysing the average oxidation state of carbon and water demand per residue, calculated using elemental abundances and stoichiometric reactions to form proteins from basis species. The authors [127] demonstrated the ability to track 1% calcium variations between adipose and breast surrogates and 2% oxygen variations between the several tissue surrogates, and a logarithmic trend between the elemental concentration of the target and the prompt gamma production induced by the irradiation of such elements. The absolute measurements of total-body calcium using prompt gamma have been reported in renal patients. It was demonstrated that proton and ion beam spectroscopy is sensitive enough for the analysis of calcification in metastases. The iodine value for the Italian heavy pig subcutaneous adipose tissue from fatty acid methyl ester profiles was calculated. The specific equations for the calculation of lipids were developed [128]. Since only few studies of chemical analysis in the human adipose tissue are reported, and these results obtained are scattered, it is impossible to draw any general conclusions.

SCANNING ELECTRON MICROSCOPY (SEM)

The morphology by scanning electron microscopy (SEM) of the adipose samples was investigated in several studies [14, 79, 129, 130]. The adipose tissue was taken from volunteer obese patients from subcutaneous, preperitoneal and visceral layers of adipose tissue (Fig. 1). For example, the SEM micrographs of subcutaneous adipose tissue layer taken from obese patients having different metabolic diseases are presented in Fig. 10. These SEM images are slightly different in comparison with the ones taken from the SAT layers of people without metabolic diseases. It can be seen from Fig. 4 that the adipose tissue samples are composed of cubes, prisms and spherically shaped granules particles less than 0.5 μm in size. These different geometric shapes are connected by solid matrix. Moreover, pores and voids can also be seen, which result probably from the different natural condition of adipose tissue. The interesting morphological feature is rarely observed bright spots in all SEM micrographs of the SAT adipose tissue picked up from different patients. These bright spots probably are associated with metabolic changes in the body of obese patients. However, only few samples contain rod- and/or stick-like individual particles 0.5–2.0 μm in size which were seen in the SEM images of the SAT layers of healthy volunteers.

The distribution of different morphological features in different layers of the lyophilised adipose tissue was also investigated [14]. The typical SEM micrographs of the adipose tissue samples obtained from the preperitoneal (PAT), subcutaneous (SAT) and visceral (VAT) layers of obese patients with different metabolic diseases are shown in Fig. 11. The obtained microstructural results
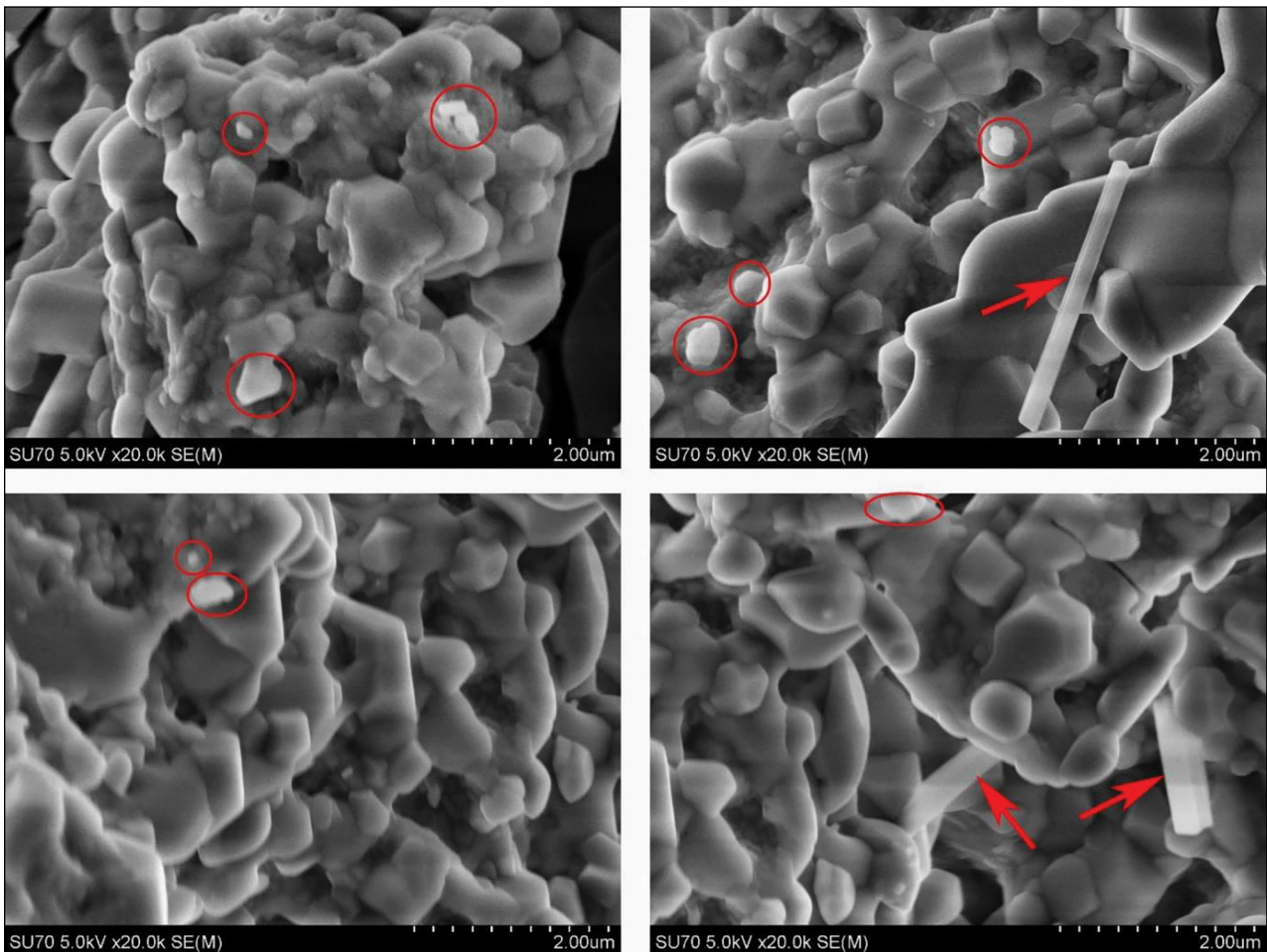

Fig. 10. SEM micrographs of the adipose tissue obtained from the subcutaneous layers of obese patients with different metabolic diseases. The bright spots are marked* [129]
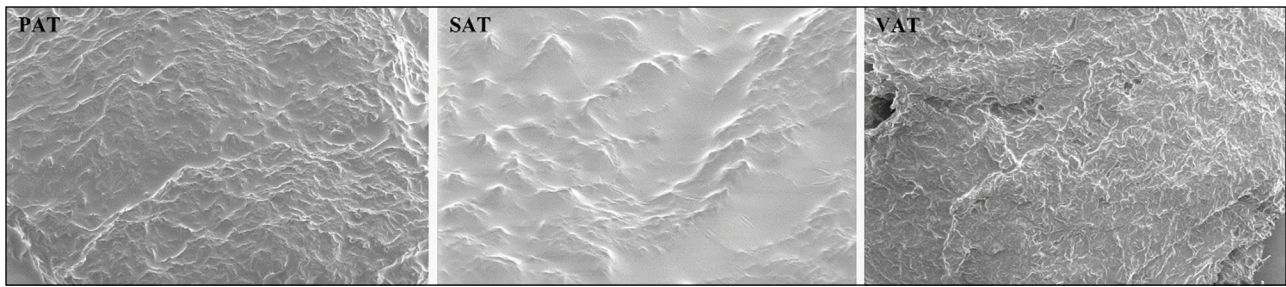
Fig. 11. Typical SEM micrographs of the lyophilised adipose tissue obtained from the preperitoneal (PAT), subcutaneous (SAT) and visceral (VAT) layers of obese patients with different metabolic diseases [14]

clearly informed that the calculated specific area of thickening and scarring of the connective tissue for the obese patients with different metabolic diseases was much larger than for obese and healthy people (Fig. 12). Besides, three different techniques were tested to construct the 3D view from the SEM images of adipose tissue [130]. The 3D reconstructed model by VisualSFM and MeshLab free available software gave the best and the most promising results. The surface was fully reconstructed and the pixel z dimension might be easily extrapolated (see Fig. 13). The reconstructed view also might be easily printed by a 3D printer which gives a new area of applications.

To study the microenvironment of bone marrow adipocyte a three-dimensional analysis of the ultrastructure with focused ion beam scanning electron microscopy (FIB-SEM) was also performed [131].

These images provided a unique opportunity to visualise the native bone marrow adipocyte within its skeletal niche and strongly implied that bone marrow adipocytes actively participate in physiologic energy partitioning and signalling within the skeletal microenvironments. The SEM results could provide an important information about the structural composition of adipose tissue layers in the human body, as well as the main microstructural features; however, the sample preparation for SEM measurements should be performed with a special care. Recently it was demonstrated that a simple method of thawing cryo-stored samples preserves ultrastructural features in electron microscopy [132]. In addition, transmission electron microscopy (TEM) was also applied to study the role of adipose tissue function in obesity [133]. Liu et al. [134] examined the morphological features of the adult and neonatal
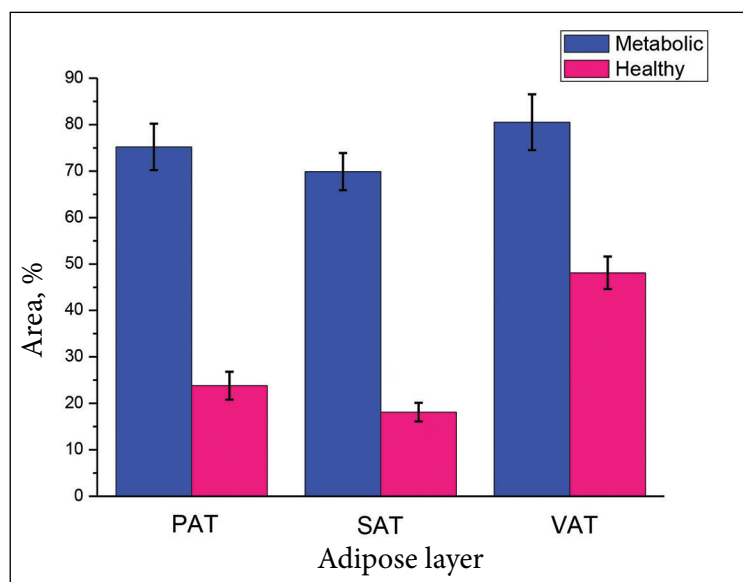

Fig. 12. Distribution of thickening of the adipose tissue obtained from the PAT, SAT and VAT layers of obese patients with and without different metabolic diseases [14]
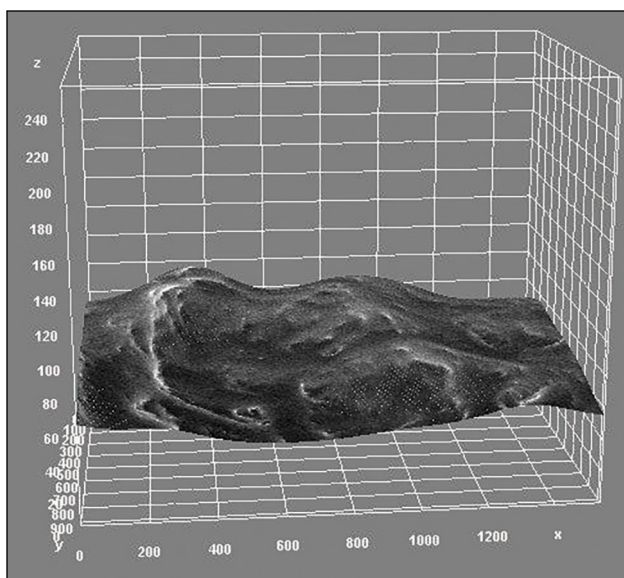
Fig. 13. Interactive 3D surface of the deeper level of subcutaneous adipose tissue [130]

adipose tissue of mice by using TEM and SEM. They found that the neonatal adipose tissue contains a smaller number and size of lipid droplets, as well as more abundant mitochondria, compared with the adult samples. The dynamic morphological changes revealed that the number and size of lipid droplets increased, but the number of mitochondria gradually decreased during the post-delivery development. Thus, careful morphological observations revealed the individual surface morphology of some adipose tissue samples taken from different patients.

Additionally, few biosensing systems were developed for the determination of different compounds presented in adipose tissue and for the investigating obesity-associated inflammation [135–138].

CONCLUSIONS

In this review, for the first time, to the best of our knowledge, the application of analytical techniques, such as gas and liquid chromatography, Fourier transform infrared (FTIR) spectroscopy, nuclear magnetic resonance (NMR) spectroscopy, elemental analysis and scanning electron microscopy (SEM) for the characterisation of adipose tissue from obese patients, was summarised. Gas and liquid chromatography are conventional methods for determining the composition of fats in the adi-

pose tissue. Liquid chromatography techniques are also very important in lipidomics research. According to the FTIR analysis results, it was concluded that the main functional groupings in the adipose tissue taken from subcutaneous, preperitoneal and visceral layers of different obese patients were different. Therefore, FTIR spectroscopy was successfully used for the analysis and direct qualitative characterisation of adipose tissue composition. The Raman spectroscopy showed even more possibilities for the analysis of the specific features of adipose tissue. It was demonstrated that the ^{1}H NMR spectra of adipose tissue samples could be used to predict the different pathologies of obese patients. The results of elemental analysis showed a various distribution of different metals in the adipose tissue of differently obese patients. It could be concluded that the results of distribution of some metals in the adipose tissue layers of people with overweight are promising for further medical observation. Also, careful morphological observations using SEM and TEM measurements revealed the individual surface morphology of adipose tissue samples taken from different patients. From the obtained results is was concluded that such characterisation of adipose tissue is an essential step for the possible prediction of the appearance of symptoms of different diseases, since recent studies have emphasised on a close relationship between the adipose tissue properties and development of fat distribution and metabolism, and different diseases. This may facilitate the future development of new prognostic tools useful for personalised treatment strategies that address problems in obesity and its complications. In summary, this review shows interesting findings, which may provide new insights into the treatment of metabolic diseases.

References

1. D. T. Villareal, C. M. Apovian, R. F. Kushner, S. Klein, *Am. J. Clin. Nutr.*, **82**, 923–934 (2005).
2. F. J. Ruiz-Ojeda, A. Anguita-Ruiza, R. Leis, C. M. Aguilera, *Ann. Nutr. Metab.*, **73**, 89–99 (2018).
3. E. Lespessailles, J. Paccou, R.-M. Javier, T. Thomas, B. Cortet, *J. Clin. Endocrinol. Metab.*, **104**, 4756–4768 (2019).
4. N. Hwalla, Z. Jaafar, *Diagnostics*, **11**, 24 (2021).

5. H. B. Kitzinger, B. Karle, *Eur. Surg.*, **45**, 80–82 (2013).

6. L. Basurto, L. Sanchez, A. Diaz, M. Valle, A. Robledo, C. Martinez-Murillo, *Thrombosis Res.*, **180**, 110–114 (2019).

7. A. Ortiz-Dosal, P. Rodil-Garcia, L. A. Salazar-Olivo, *Biomarkers*, **24**, 499–509 (2019).

8. J. R. Larsen, L. Dima, C. U. Correll, P. Manu, *Expert Rev. Clin. Pharmacol.*, **11**, 397–410 (2018).

9. T. Grewal, C. Enrich, C. Rentero, C. Buechler, *Int. J. Mol. Sci.*, **20**, 3449 (2019).

10. C. Koliaki, S. Liatis, A. Kokkinos, *Metabolism Clin. Exper.*, **92**, 98–107 (2019).

11. H. Li, A. Chen, L. Shu, et al., *Genes Cells*, **19**, 793–802 (2014).

12. B. A. Evans, J. Merlin, T. Bengtsson, D. S. Hutchinson, *Br. J. Pharmacol.*, **176**, 2416–2432 (2019).

13. Q. Zhu, B. J. Glazier, B. C. Hinkel, et al., *Int. J. Mol. Sci.*, **20**, 2707 (2019).

14. G. Brimas, R. Skaudzius, V. Brimiene, R. Vaitkus, A. Kareiva, *Medic. Hypotheses*, **136**, 109526 (2020).

15. V. Mohamed-Ali, J. H. Pinkney, S. W. Coppack, *Int. J. Obes. Relat. Metab. Disord.*, **22**, 1145–1158 (1998).

16. L. Luo, M. Liu, *J. Endocrinol.*, **231**, R77–R99 (2016).

17. S. Russo, M. Kwiatkowski, N. Govorukhina, R. Bischoff, B. N. Melgert, *Front. Immunol.*, **12**, 746151 (2021).

18. C. M. Ahlberg, L. N. Schiermiester, J. T. Howard, C. R. Calkins, M. L. Spangler, *Meat Sci.*, **98**, 804–814 (2014).

19. M. Ebadi, V. E. Baracos, O. F. Bathe, L. E. Robinson, V. C. Mazurak, *Clin. Nutrit.*, **35**, 1347–1353 (2016).

20. J. P. Bastard, B. Feve, *Physiology and Physiopathology of Adipose Tissue*, Springer, Verlag, France (2013).

21. A. Selovic, J. Sarac, S. Missoni, *J. Matern. Fetal Neonatal Med.*, **29**, 2131–2137 (2016).

22. B. Hacihamdioglu, G. Ocal, M. Berberoglu, et al., *Ultrasound Med. Biol.*, **40**, 871–876 (2014).

23. A. T. Cote, A. A. Phillips, K. C. Harris, G. G. S. Sandor, C. Panagiotopoulos, A. M. Devlin, *Arterioscler. Thromb. Vasc. Biol.*, **35**, 1038–1044 (2015).

24. M. De Spiegeleer, E. De Paepe, L. Van Meulebroek, I. Gies, J. De Schepper, L. Vanhaecke, *Mol. Med.*, **27**, 145 (2021).

25. K. G. Kahl, J. Herrmann, B. Stubbs, et al., *Progr. Neuropsychopharmacol. Biolog. Psychiatry*, **72**, 30–35 (2017).

26. C. Pisitsak, J. G. H. Lee, J. H. Boyd, H. O. Coxson, J. A. Russell, K. R. Walley, *Critic. Care Med.*, **44**, 1966–1973 (2016).

27. G. E. Shearrer, M. J. Daniels, C. M. Toledo-Corral, M. J. Weigensberg, D. Spruijt-Metz, J. N. Davis, *Physiol. Behav.*, **167**, 188–193 (2016).

28. S. J. Yu, W. Kim, D. Kim, et al., *Medicine*, **94**, e2159 (2015).

29. E. S. Wahyuni, I. W. A. Wiyasa, N. Nurdiana, *Middle East Fertil. Soc. J.*, **21**, 259–263 (2016).

30. M. Z. Zhang, T. Hu, S. Y. Zhang, L. Zhou, *Sci. Rep.*, **5**, 18495 (2015).

31. Y.-C. Tsao, J.-Y. Chen, W.-C. Yeh, Y.-S. Peng, W.-C. Li, *BMJ Open*, **0**, e017117 (2017).

32. J. C. Brown, M. O. Harhay, M. N. Harhay, *Insights*, **12**, 1–3 (2019).

33. T. Iwase, T. Sangai, H. Fujimoto, et al., *Breast Cancer Res. Treatm.*, **179**, 435–443 (2020).

34. S. Casteras, A. Abdul-Wahed, M. Soty, et al., *Diabetologia*, **59**, 2645–2653 (2016).

35. D. H. Ipsen, P. Tveden-Nyborg, J. Lykkesfeldt, *Curr. Obes. Rep.*, **5**, 405–412 (2016).

36. S. Wang, X. Liu, Q. Chen, C. Liu, C. Huang, X. Fang, *BMC Anesthesiol.*, **17**, 118 (2017).

37. C. Aguiar, J. MacLeod, A. Yip, et al., *BMJ Open*, **9**, e023418 (2019).

38. S. Russo, M. Kwiatkowski, N. Govorukhina, R. Bischoff, B. N. Melgert, *Front. Immunol.*, **12**, 746151 (2021).

39. A. Feola, S. Ricci, S. Kouidhi, et al., *J. Cell. Physiol.*, **232**, 69–77 (2017).

40. M. A. Kasinska, J. Drzewoski, A. Sliwinska, *Arch. Med. Sci.*, **12**, 1293–1301 (2016).

41. T. Y. Kim, A. L. Schafer, *Curr. Osteoporos. Rep.*, **14**, 337–344 (2016).

42. A. Chirita-Emandi, M. C. Papa, L. Abrudan, et al., *Rom. J. Morphol. Embryol.*, **58**, 115–123 (2017).

43. J. T. Brenna, M. Plourde, K. D. Stark, P. J. Jones, Y.-H. Lin, *Am. J. Clin. Nutr.*, **108**, 211–227 (2018).

44. L. R. S. Abreu, M. K. Shirley, N. P. Castro, et al., *PLOS ONE*, **14**, e0221971 (2019).

45. F. C. Gabriel, G. Fantuzzi, *Nutrition Res.*, **72**, 18–35 (2019).

46. M. J. Trites, R. D. Clugston, *Lipids Health Dis.*, **18**, 204 (2019).

47. J. Bliton, D. Sussman, R. M. Summers, J. H. Yao, *Current Med. Imag.*, **13**, 364–382 (2017).

48. Z. Bahadoran, S. Jeddi, S. Gheibi, P. Mirmiran, K. Kashfi, A. Ghasemi, *EXCLI J.*, **19**, 972–983 (2020).

49. I. Liakh, T. Sledzinski, L. Kaska, P. Mozolewska, A. Mika, *Molecules*, **25**, 5307 (2020).

50. A. Bar, A. Kieronska-Rudek, B. Proniewski, et al., *J. Am. Heart Assoc.*, **9**, e016929 (2020).

51. F. Castriota, L. Rieswijk, S. Dahlberg, et al., *Env. Health Perspect.*, **128**, 016001 (2020).

52. A. A. Tinkov, O. P. Ajsuvakova, T. Filippini, et al., *Biomolecules*, **10**, 658 (2020).

53. A. V. G. Ramirez, D. R. Filho, L. B. P. C. de Sa, *Curr. Diabetes Rev.*, **17**, e081020184730 (2021).

54. M. Aslan, *Mini Rev. Org. Chem.*, **18**, 3–10 (2021).

55. Z. Suna, B. D. Gepner, S.-H. Leea, et al., *Acta Biomater.*, **129**, 188–198 (2021).

56. S. Bamba, O. Inatomi, K. Takahashi, et al., *Inflamm. Bowel Dis.*, **27**, 1435–1442 (2021).

57. J.-B. Bouillon-Minois, M. Trousselard, et al., *Nutrients*, **13**, 3350 (2021).

58. S. Vedantham, L. Shi, A. Karellas, *Phys. Med. Biol.*, **59**, 6387–6400 (2014).

59. J. Liu, C. Zhang, B. Zhang, et al., *Cells*, **9**, 201 (2020).

60. W. Stoffel, F. Chu, E. H. Ahrens, *Anal. Chem.*, **31**, 307–308 (1959).

61. N. Quinete, T. Schettgen, J. Bertram, T. Kraus, *Anal. Bioanal. Chem.*, **406**, 6151–6164 (2014).

62. F. Bevalot, C. Bottinelli, N. Cartiser, L. Fanton, J. Guitton, *J. Anal. Toxicol.*, **38**, 256–264 (2014).

63. D. Lu, C. Feng, Y. Lin, et al., *Chemosphere*, **114**, 327–336 (2014).

64. M. Wolters, C. Dering, A. Siani, et al., *PLoS ONE*, **12**, e0181485 (2017).

65. Z. P. Yali, A. P. Jadid, L. A. Samin, *Int. J. Environ. Sci. Technol.*, **14**, 2357–2366 (2017).

66. A. M. Astudillo, C. Meana, C. Guijas, et al., *J. Lipid Res.*, **59**, 237–249 (2018).

67. V. Poškus, V. Vičkačkaitė, G. Brimas, *Chemija*, **27**, 179–184 (2016).

68. V. Poškus, V. Vičkačkaitė, J. Dargytė, G. Brimas, *Chemija*, **29**, 49–56 (2018).

69. J. P. Arrebola, J. Pumarega, M. Gasull, et al., *Environm. Res.*, **122**, 31–37 (2013).

70. R. A. Ghazala, A. El Medney, A. Meleis, P. Mohie El dien, H. Samir, *Biomed. Chromatogr.*, **34**, e4743 (2020).

71. J. Hamulka, J. Brys, A. Gorska, M. Janaszek-Mankowska, M. Gornicka, *Appl. Sci.*, **11**, 10029 (2021).

72. R. Tessari, E. Mazzotta, F. Blasi, et al., *Large Anim. Rev.*, **27**, 187–193 (2021).

73. M. Lange, Z. Ni, A. Criscuolo, M. Fedorova, **82**, 77–100 (2019).

74. R. Anlicoara, A. A. B. Ferraz, K. da P. Coelho, et al., *Obes. Surg.*, **24**, 1487–1491 (2014).

75. E. Bartosinska, J. Jacyna, A. Borsuk-De Moor, et al., *Talanta*, **176**, 108–115 (2018).

76. M. Guan, D. Dai, L. Li, et al., *Talanta*, **172**, 206–214 (2017).

77. V. C. O. Lima, A. B. S. Luz, M. do Socorro M. Amarante, et al., *Obes. Facts*, **14**, 357–369 (2021).

78. O. Awosemo, H. Neelakantan, S. Watowich, et al., *Biomed. Anal.*, **204**, 114255 (2021).

79. B. Buckus, G. Brimas, A. Stasinskas, et al., *Chemija*, **26**, 98–106 (2015).

80. F. K. Baloglu, O. Baloglu, S. Heise, G. Brockmann, F. Severcan, *J. Biophotonics*, **10**, 1345–1355 (2017).

81. E. Aboualizadeh, O. T. Carmichael, P. He, D. C. Albarado, C. D. Morrison, C. J. Hirschmugl, *Front. Endocrinol.*, **8**, 121 (2017).

82. I. Bikulčienė, L. Vasiliauskaitė, Z. A. Kučinskienė, A. Kaminskas, V. Hendrixson, *Med. Sci. Monit.*, **24**, 818–826 (2018).

83. D. Ami, P. Mereghetti, A. Foli, et al., *Anal. Chem.*, **91**, 2894–2900 (2019).

84. K. Yu, H. Zhang, Y. Liu, et al., *Microchem. J*, **164**, 105977 (2021).

85. S. Liyanage, R. S. Dassanayake, A. Bouyanfif, et al., *MethodsX*, **4**, 118–127 (2017).

86. T. Ansari, A. Southgate, I. Obiri-Yeboa, et al., *Stem Cells Develop.*, **29**, 314–326 (2020).

87. F. Munir, S. G. Musharraf, S. T. H. Sherazi, M. I. Malik, M. I. Bhanger, *Turk. J. Chem.*, **43**, 1098–1108 (2019).

88. M. Y. Bekhit, B. Grung, S. A. Mjos, *Appl. Spectrosc.*, **68**, 1190–1200 (2014).

89. M. Motoyama, I. Nakajima, H. Ohmori, G. Watanabe, K. Sasaki, *JARQ*, **52**, 17–22 (2018).

90. F. Tao, M. Ngadi, *Crit. Rev. Food Sci. Nutrit.*, **58**, 1565–1593 (2018).

91. I. Y. Yanina, Y. I. Svenskaya, E. S. Prikhozhdenko, *J. Biophotonics*, **11**, e201800058 (2018).

92. K. St-Arnaud, K. Aubertin, M. Strupler, et al., *Med. Phys.*, **45**, 328–339 (2018).

93. F. Daoust, T. Nguyen, P. Orsini, et al., *J. Biomed. Optics*, **26**, 022911-1-18 (2021).

94. C. Blücher, C. Zilberfain, T. Venus, et al., *Analyst*, **144**, 5558 (2019).

95. E. Swiderska, M. Podolska, J. Strycharz, et al., *Nutrients*, **11**, 1835 (2019).

96. P. N. Paramitha, R. Zakaria, A. Maryani, et al., *Mol. Sci.*, **22**, 7378 (2021).

97. Z. Majka, K. Czamara, P. Wegrzyn, et al., *Analyst*, **146**, 270 (2021).

98. P. Meksiarun, B. B. Andriana, H. Matsuyoshi, H. Sato, *Sci. Rep.*, **6**, 37068 (2016).

99. M. Troyanova-Wood, C. Gobbell, Z. Meng, A. A. Gashev, V. V. Yakovlev, *J. Biophotonics*, **10**, 1694–1702 (2017).

100. C. T. Kucha, L. Liu, M. O. Ngadi, *Sensors*, **18**, 377 (2018).

101. G. Donjuan-Loredo, R. Espinosa-Tanguma, F. Leon-Bejarano, et al., *Appl. Spectrosc*, **75**, 1189–1197 (2021).

102. A. Zajac, L. Dyminska, J. Lorenc, M. Ptak, J. Hanuza, *Spectroscopy Lett.*, **51**, 81–88 (2018).

103. M. Troyanova-Wood, C. Gobbell, Z. Meng, O. Gasheva, A. A. Gashev, V. V. Yakovlev, *J. Biophotonics*, **14**, e202000269 (2021).

104. C. Blay, P. Haffray, J. D'Ambrosio, et al., *BMC Genomics*, **22**, 788 (2021).

105. C. Corden, R. Boitor, I. Notingher, *J. Phys. D Appl. Phys.*, **54**, 504003 (2021).

106. G. Donjuan-Loredo, R. Espinosa-Tanguma, M. G. Ramirez-Elias, *Appl. Spectrosc. Rev.* (2021) [https://doi.org/10.1080/05704928.2021.1944175].

107. B. Jin, L. P. Liu, S. X. Zhang et al., *Metabol. Syndr. Relat. Disord.*, **15**, 439–449 (2017).

108. I. J. Neelanda, C. Hughes, C. R. Ayers, C. R. Malloy, E. S. Jin, *Metabolism*, **67**, 80–89 (2017).

109. M. Gajdosik, L. Hinger, A. Skoch, et al., *J. Magn. Reson. Imaging.*, **50**, 71–82 (2019).

110. D. Le Duc, C.-C. Lin, Y. Popkova, et al., *Int. J. Obes.*, **45**, 565–576 (2021).

111. A. N. Torres, L. Tavares, M. J. Pereira, J. W. Eriksson, J. G. Jones, *NMR Biomed.*, e4632 (2021).

112. A. Paul, S. Kumar, A. Raj, *Metabolomics*, **14**, 119 (2018).

113. A. F. Soares, J. Paz-Montoya, H. Lei, M. Moniatte, R. Gruetter, *NMR Biomed.*, **30**, e3761 (2017).

114. C. Carpene, J. Mercader, S. Le Gonidec, *Br. J. Pharmacol.*, **175**, 2428–2440 (2018).

115. S. O. Senera, U. Ozgen, S. Kanbolat, *S. Afr. J. Bot.*, **141**, 243–254 (2021).

116. C. J. Fallone, A. G. Tessier, C. J. Field, A. Yahya, *NMR Biomed.*, **34**, e4455 (2021).

117. S. Furse, D. S. Fernandez-Twinn, B. Jenkins, *Anal. Bioanal. Chem.*, **412**, 2851–2862 (2020).

118. J.-L. Jung, G. Simon, E. Alfonsi, *PLoS One*, **12**, e0180597 (2017).

119. A. Meusel, Y. Popkova, D. Dannenberger, J. Schiller, *Food Anal. Methods*, **10**, 2497–2506 (2017).

120. J. O. Aleman, N. A. Bokulich, J. R. Swann, *J. Transl. Med.*, **16**, 244 (2018).

121. J. M. Moreno-Navarrete, M. Serino, V. Blasco-Baque, et al., *Mol. Nutr. Food Res.*, **62**, 1700721 (2018).

122. A. B. Granado-Serrano, M. Martin-Gari, V. Sanchez, et al., *Sci. Rep.*, **9**, 1772 (2019).

123. K. Oshakbayev, B. Dukenbayeva, G. Togizbayeva, et al., *BBA Clin.*, **8**, 14–19 (2017).

124. E. M. Johnston, E. Dao, M. J. Farquharson, et al., *X-Ray Spectrom.*, **48**, 432–437 (2019).

125. A. Kizalaite, V. Brimiene, G. Brimas, et al., *Trace Elem. Res.*, **189**, 10–17 (2019).

126. J. M. Dick, *PeerJ*, **5**, e3421 (2017).

127. P. M. Martins, R. D. Bello, B. Ackermann, et al., *Sci. Rep.*, **10**, 7007 (2020).

128. D. P. Lo Fiego, G. Minelli, L. A. Volpelli, A. Ulrici, P. Macchioni, *Meat Sci.*, **122**, 132–138 (2016).

129. R. Skaudžius, M. Misevičius, V. Brimienė, M. Beniušė, G. Brimas, A. Kareiva, *Chemija*, **29**, 67–80 (2018).

130. E. Brimas, R. Skaudžius, G. Brimas, A. Selskis, R. Ramanauskas, A. Kareiva, *Chemija*, **33**, 7–11 (2022).

131. H. Robles, S. J. Park, M. S. Joens, J. A. J. Fitzpatrick, C. S. Craft, E. L. Scheller, *Bone*, **118**, 89–98 (2019).

132. M. Galhuber, N. Kupper, G. Dohr, et al., *Cell Biol.*, **155**, 593–603 (2021).

133. F. Wu, X. Yang, M. Hu, et al., *Phytomedicine*, **76**, 153258 (2020).

134. J. Liu, C. Zhang, B. Zhang, et al., *Cells*, **9**, 201 (2020).

135. J. Zhu, J. He, M. Verano, et al., *Lab. Chip.*, **18**, 3550 (2018).

136. M. Jafari, M. Hasanzadeh, R. Karimian, N. Shadjou, *Microchem. J.*, **147**, 741–748 (2019).

137. K. L. Westmacott, A. P. Crew O. Doran, J. P. Hart, *Biosens. Bioelectron.*, **150**, 111837 (2020).

138. E. Santos, M. F. F. Vara, M. Ranciaro, W. Strasse, G. N. N. Neto, P. Nohama, *J. Biomechan.*, **122**, 110456 (2021).

Edvardas Brimas, Rimantas Raudonis, Aivaras Kareiva

ANALIZĖS METODAI, NAUDOJAMI SPECIFINĖMS SU NUTUKIMU SUSIJUSIŲ BIOLOGINIŲ AUDINIŲ YPATYBĖMS APIBŪDINTI: APŽVALGA

S a n t r a u k a

Nutukimas tapo pasauline pandemija, dėl kurios išsivysto daugelis įprastų sutrikimų, tokių kaip 2-ojo tipo diabetas, metabolinis sindromas, širdies ir kraujagyslių ligos, ir netgi padidėja susirgimų vėžiu rizika. Šiame tyrime išnagrinėti keli analizės metodai, tokie kaip dujų ir skysčių chromatografija, Furjė transformacijos infraraudonųjų spindulių (FTIR) ir Ramano spektroskopijos, branduolinio magnetinio rezonanso (BMR) spektroskopija, skenuojanti elektronų mikroskopija (SEM) ir elementų analizė, kaip pagrindinės priemonės, naudojamos riebalinio audinio mėginiams apibūdinti. Šioje apžvalgoje daugiausia dėmesio skirta nustatyti ryšiui tarp gautų rezultatų, kurie suteikia informacijos apie riebalinio audinio sluoksnių cheminę ir struktūrinę sudėtį žmogaus organizme bei pagrindines mikrostruktūrines ypatybes, ir nutukimo. Įrodyta, kad šie analizės metodai yra nepakeičiami instrumentai tiriant kai kuriuos žmogaus riebalinio audinio ypatumus, identifikuojant cheminę sudėtį ir struktūrinius požymius. Be to, apibendrinti rezultatai leidžia daryti išvadą, kad toks riebalinio audinio apibūdinimas yra esminis žingsnis numatant galimą įvairių ligų simptomų atsiradimą.